Journal of Analytical and Applied Pyrolysis 180 (2024) 106545

Contents lists available at ScienceDirect

Journal of Analytical and Applied Pyrolysis

journal homepage: www.elsevier.com/locate/jaap

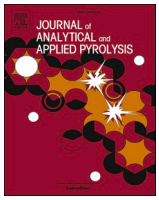

Production of sludge biochar by steam pyrolysis and acid treatment: Study of the activation mechanism and its impact on physicochemical properties

Irene Sierra [a,*], Eva Epelde [b], José L. Ayastuy [b], Unai Iriarte-Velasco [a]

[a] Department of Chemical Engineering, Faculty of Pharmacy, University of the Basque Country (UPV/EHU), Vitoria-Gasteiz, Spain
[b] Department of Chemical Engineering, Faculty of Science and Technology, University of the Basque Country (UPV/EHU), Leioa, Spain

ARTICLE INFO

Keywords:
Sewage sludge
Steam
HCl
Biochar
Activation mechanism
Acid activation

ABSTRACT

This study addresses the preparation of sludge biochar through a procedure that combines steam pyrolysis in a wide range of temperature (500–900 ºC) and acid treatment with HCl (performed before or after the pyrolysis). The acid washing after the pyrolysis maximizes BET surface area due to pore unblocking, thus making visible the pore structure generated. The drawback of the acid washing is the lower yield obtained (compared to the acid pretreatment), as well as the loss of the magnetic properties of sludge biochar. The acid pretreatment requires temperatures above 700 ºC to have a beneficial effect, due to the occurrence of additional reactions of the incorporated HCl with sludge constituents. The pretreatment results in materials with a high degree of microporosity. Among the reactions favoured, of interest is the development of magnetite in the whole temperature range. The activation protocol used in this study (especially the procedure that includes the acid pretreatment) is effective to generate biochar with magnetic properties through the transformation of the Fe introduced during the water treatment process, without adding a source of Fe. The presence of magnetite is an advantage for the reuse of sludge biochars in wastewater treatment.

1. Introduction

Sewage sludge is the unavoidable residue from wastewater treatment plants, which are used to purify the wastewater produced in households, industry and public facilities. The composition of sewage sludge is affected by different parameters including the source, the operations carried out during the treatment and the season, thus leading to a high variability [1]. Sewage sludge is a complex and heterogeneous mixture of water, microorganisms, undigested organic matter and inorganic substances. The organic matter represents approximately 60 wt% on a dry basis, and it is mainly composed of bacterial constituents such as proteins, peptides, lipids, polysaccharides and undigested organic material [2]. Sewage sludge also contains nitrogen and phosphorus in different forms, together with high concentrations of inorganic salts including anions (carbonates, phosphates, sulfates and nitrates), heavy metals (such as Zn, Pb, Ni, Cd, Cr, Cu, As and Hg) and other elements (e.g. Si, Al, K, Na, Ca and Mg) [3]. Since sewage sludge is composed of substances responsible for the toxic and pathogenic nature of wastewater, its management is an issue of particular concern.

The traditional options to manage sewage sludge include land filling, incineration, ocean discharge and composting [4]. Nevertheless, owing to the increasingly stringent environmental regulations to avoid secondary pollution, along with the growing demand for the recovery of energy and materials from sludge (in the context of sustainability and circular economy), there is an increasing interest in the search of alternative treatment methods. Among these strategies, the treatment of sewage sludge by means of a thermochemical procedure in an oxygen-limited atmosphere (pyrolysis) represents an economical and environmentally friendly alternative. The solid fraction obtained (biochar or sludge carbon) is a material with a wide range of applications due to its high carbon content, porosity, cation exchange ability and stability, as well as to its functional groups [3]. Biochar derived from sludge can be used in water and wastewater treatment in different ways [5]: (i) as an adsorbent for the removal of many contaminants such as dyes, heavy metals, emerging pollutants (e.g. phenolic compounds and pharmaceuticals) and other compounds (e.g. phosphates and nitrates), (ii) as a catalyst in advanced oxidation processes based on persulfate activation and Fenton reaction to degrade recalcitrant pollutants, (iii) as an electrode in electrochemical processes. Sewage sludge-derived biochar can also be used to remove gas pollutants such as H_2S, SO_2 and NO_x [6], and as a soil amendment for several purposes: soil fertilization, water retention, pollutant immobilization and carbon sequestration [7].

* Corresponding author.
E-mail address: irene.sierra@ehu.eus (I. Sierra).

https://doi.org/10.1016/j.jaap.2024.106545
Received 5 March 2024; Received in revised form 23 April 2024; Accepted 11 May 2024
Available online 15 May 2024

Other potential applications are the storage of gases such as H_2, O_2 or CH_4 through adsorption, the use of biochar as a solid biofuel to generate energy through combustion in the power or heat industry, or its use as catalyst or catalyst support [5,6].

The optimal physicochemical properties of biochar depend on the desired application. For example, sludge carbons with high porosity and large specific surface area are preferred for electrochemical and catalytic processes, gas storage and pollutant removal in both liquid and gas phase, whereas the composition (such as the amount of heavy metals, nitrogen and phosphorus) is crucial for its use in soil amendment. These properties vary according to sludge source (primary, secondary, anaerobic digestion and dewatering process) and can be adjusted by means of the preparation procedure [8].

The usual preparation procedure of sludge carbon starts with the drying of wet sewage sludge, followed by either physical or chemical activation. Physical activation usually comprises two stages [9]: a pre-carbonization of sludge at intermediate temperature (400–700 ºC) to break down the cross-linkage between carbon atoms, followed by an activation step (pyrolysis) with a gas such as CO_2 or steam at high temperature. The most common activation gas is steam, owing to its capacity to produce a wide pore size distribution [10]. Regarding the chemical activation, the precursor (either sludge or pre-carbonized sludge) is mixed with a chemical reagent (an acid, an alkaline compound or a salt) and then is heated up to a high temperature under an inert atmosphere.

Many studies have shown the advantages of performing an acid treatment in the preparation of biochar: (i) removal of inorganic matter, thus leading to an increase in the porosity due to the opening of pore channels [6], (ii) increase in the calorific value due to the reduction in the ash content [6], (iii) enhancement in metal ions uptake due to the replacement of exchangeable cations by H^+ ions [11], (iv) introduction of functional groups on the surface of biochar [3], (v) removal of certain leachable compounds, thus reducing the risk of leaching in water treatment [12]. Nevertheless, the optimum acid washing sequence (before or after the pyrolysis step) remains unclear, since the studies comparing pre- and post-washing are scarce. In this regard, although it has been reported that the post-washing may be less effective because the thermal treatment increases the stability of the inorganic fraction (i.e., lowers its propensity towards leaching) [12], our previous comprehensive study revealed that post-washing was more effective in increasing the porosity of biochar prepared by pyrolysis of sewage sludge with CO_2 [13]. Furthermore, the acid washing after the pyrolysis has the advantage of removing the products formed during the activation step from the new interstices formed, whereas an excessive removal of minerals before the pyrolysis may eliminate the catalytic activity of the material during the pyrolysis [14,15]. However, when the acid washing is performed before the pyrolysis, sewage sludge is subjected to a combined physical and chemical activation process (or a multiple modification), thus taking advantage of the reactions and processes favoured by the acid during the pyrolysis. The combined activation is a promising preparation procedure of biochar not sufficiently studied [3].

The knowledge of the reactions and processes that take place during the pyrolysis of sludge and their impact on the physicochemical properties of biochar is essential to configure a material with optimal characteristics for the desired application. Unfortunately, the literature regarding this issue is scarce, and the activation mechanism should be studied at a deeper level [6]. To the best of the authors' knowledge, the only comprehensive study that includes a detailed activation mechanism is our previous investigation of sludge biochar prepared by alkaline treatment with NaOH and K_2CO_3 in CO_2 atmosphere [16]. Nevertheless, there is no detailed study on the mechanism of steam activation, nor on the mechanism of acid activation.

This study addresses the preparation of sludge carbon through a procedure that combines pyrolysis with steam in a wide range of temperature (500–900 ºC, at intervals of 100 ºC) and acid treatment with HCl. The temperature range selected is ascribed to medium-low, intermediate and high temperature pyrolysis [17]. The highest temperature has been limited to 900 ºC to avoid the deterioration of the textural properties that takes place at too high temperatures. Indeed, for steam pyrolysis it has been reported that temperatures above 850 ºC result in the decrease of BET surface area [9]. The preparation method proposed does not require the usual pre-carbonization step [18] (the precursor is dry sewage sludge, not biochar), thus resulting in an important reduction of the preparation cost, due to the higher yield obtained, and the lower operational cost and processing time. The effect of the sequence of the acid treatment has been studied, since it is not sufficiently clear. The investigation is focused on analyzing the structural rearrangements and the changes in the chemical composition of the prepared materials, using numerous techniques: elemental analysis, ICP-MS, N_2 adsorption-desorption, pH, ash content, FTIR, XRD, SEM and EDX. Finally, based on the characterization results of sludge biochar, as well as on our previous experience, a comprehensive and detailed activation mechanism has been proposed. This mechanism will be helpful to design activation protocols for materials derived from sewage sludge with tailored physicochemical properties for use in specific fields. Moreover, since carbon is one of the constituents of sewage sludge, the activation mechanism will help to improve the knowledge in the fundamentals of the activation process of any carbonaceous precursor.

2. Materials and methods

2.1. Raw material

Biochar was prepared from anaerobically digested and dewatered sewage sludge collected from an urban wastewater treatment plant. It can be assumed that it is as a well stabilized sewage sludge, with a low degree of polymerization and aromatization [13]. The proximate analysis of sewage sludge evidences a high water content (73.3 wt%).

2.2. Preparation of sludge carbon

Raw sewage sludge was subjected to a drying step in a convection oven (48 h at 105 ºC), in order to get more accurate and reproducible results on a dry basis. Moreover, it has been reported in the literature that the pre-drying step has a beneficial effect on the development of the porous structure. Lu et al. [19] reported an important increase in BET surface area after drying raw sewage sludge at high temperature (110 ºC), compared to non-dried samples. This increase was attributed to a preliminary development of the micropore structure during the drying step.

Dried sewage sludge (precursor) was ground using a mortar and sieved, and particles within the 0.5–1.0 mm size range were selected. Three different preparation procedures were investigated: (i) pyrolysis in steam atmosphere; (ii) application of the acid treatment before the pyrolysis in steam atmosphere (thereafter referred as acid pretreated); and (iii) application of the acid treatment after the pyrolysis with steam (thereafter referred as acid washed). Acid-pretreated samples were not rinsed with water before the pyrolysis. Therefore, these samples were subjected to a combined physical and chemical activation process.

The thermal treatment (conventional pyrolysis) was conducted in a quartz tube furnace, under a steam flow (0.11 mol min^{-1}). Temperature was increased from room temperature up to 500–900 ºC. The selected heating rate (15 ºC min^{-1}) is among the values corresponding to slow pyrolysis (6–60 ºC min^{-1}), since this preparation method provides the maximum yield of solid biochar [20]. Samples were maintained at the final temperature for 30 min, and then cooled down under a flow of N_2.

To carry out the acid treatment, the impregnation ratio was established at 60 mmol $g^{-1}_{precursor}$ (dry sewage sludge). This ratio is within the normal range used for the chemical activation of sewage sludge [13,21] and ensures sufficient interaction between the reagent and the precursor. The acid treatment was performed adding 1 g of the precursor to 20 cm^3 of a HCl solution (3 M). The solutions were introduced in 50 cm^3

borosilicate amber glass vials and stirred at 150 rpm in a reciprocating shaker at room temperature (20 ± 2 ºC) for 48 h, to ensure the access of the agent to the interior of the particles. Samples were then filtered, transferred to a convection oven and dried at 80 ºC for 24 h.

The samples of sludge carbon prepared by pyrolysis in steam atmosphere (SCS) were coded based on the temperature: SCS-500, SCS-600, SCS-700, SCS-800 and SCS-900. The samples subjected to acid treatment were coded according to temperature and sequence, either prior to (P) or after (A) the pyrolysis: P-SCS-500, P-SCS-600, P-SCS-700, P-SCS-800 and P-SCS-900 (acid pretreatment + pyrolysis); SCS-A-500, SCS-A-600, SCS-A-700, SCS-A-800 and SCS-A-900 (pyrolysis + acid washing). The obtained samples of biochar were washed with distilled water until a constant pH was reached.

2.3. Characterization

The precursor and a sample of the precursor impregnated with HCl were subjected to thermogravimetric analysis (TG) in a thermobalance (T.A. Instruments SDT 2960) under inert atmosphere (nitrogen).

Elemental analysis was performed using a CHNS analyzer (Euro-Vector EA-3000). The total concentration of heavy metals (Cr, Ni, Cu, Zn and Pd) was determined by a high performance Inductively Coupled Plasma Mass Spectrometer (ICP-MS, 7500ce Agilent Technologies). Prior to heavy metal determination, samples were microwave digested (Speedwave Four, Berghof) using an acid mixture (HNO_3:HF = 3:1).

The textural properties of sludge biochar were determined by N_2 adsorption/desorption at 77 K (ASAP 2010, Micromeritics). Prior to measurements, samples were outgassed under N_2 flow at 200 ºC for 15 h. Specific surface area was determined using the Brunauer-Emmett-Teller (BET) method. Surface area and pore volume in the mesopore and macropore range were obtained using the Barrett, Joyner & Halenda (BJH) method, while values in the micropore range were calculated based on the t-plot method.

pH was determined following the method described by Tessmer et al. [22]. The ash content was measured by heating the samples under air atmosphere for 1 h at 815 ºC (UNE 32004 standard).

The chemical composition and surface properties of the materials were analyzed by a scanning electron microscope (JEOL JSM-7000 F) equipped with energy dispersive X-ray detector (EDX).

Fourier transform infrared (FTIR) measurements were carried out by means of a Thermo Nicolet 6700 equipment in the absorbance mode, using the KBr self-supported pellet technique. Spectra were collected in the 400–4000 cm^{-1} range with a resolution of 2 cm^{-1}. X-ray powder diffraction patterns were collected using a Philips X'pert PRO automatic diffractometer operating at 40 kV and 40 mA, in theta-theta configuration, secondary monochromator with Cu-Kα radiation (λ = 1.5418 Å; 1 Å = 10^{-10} m) and a PIXcel solid state detector (active length in 2θ = 3.347º). Data were collected from 5 to 90° 2θ (step size = 0.026 and time per step = 1000 s) at RT. A fixed divergence and antiscattering slit giving a constant volume of sample illumination were used.

3. Results and discussion

3.1. Production yield of sludge biochar

Table 1 summarizes the results of ash content and production yields (partial and overall) for the prepared samples of sludge biochar. The yield of the pyrolysis or physical activation with steam (Y_{phys}) was calculated from sample weight before and after the treatment. The yield of the acid treatment (Y_{acid}) was obtained by dividing the mass of the sample after and before the treatment with HCl. Finally, the overall yield of sludge carbon (Y_{SC}) was obtained as the product of the aforementioned individual yields.

The activation temperature leads to a decrease in Y_{phys}, as expected, whereas the ash content increases. These results are a consequence of the higher decomposition, volatilization or gasification of sewage sludge constituents and/or incorporated species with increasing temperature, thus resulting in the concentration of the mineral constituents. It is remarkable that Y_{phys} is lower for the acid pretreated samples (P-SCS series), compared to samples subjected to steam activation only, which is partly attributed to the removal of non-volatile matter by the acid. Moreover, the acid pretreated samples are subjected to a combined physical and chemical activation process, which may result in the occurrence of additional reactions during the pyrolysis. Note that Y_{acid} is higher when the acid is applied prior to the thermal step (66 wt% vs. approx. 50 wt% for after-washed samples), thus leading to a higher overall yield. This result evidences the higher extractive capacity of the acid washing when it is performed after the steam activation although it has the drawback of the lower yield obtained.

3.2. Characterization of sludge biochars

3.2.1. Textural properties

Table 2 summarizes the textural properties of the prepared samples of sludge biochar, and Fig. 1 depicts the pore area distribution. It is observed that the materials possess a hierarchical porous structure, with pores in the micro-, meso- and macropore range.

Regarding the samples prepared by steam activation only (SCS series), the BET surface area (S_{BET}) increases with temperature, and thus, the highest value is obtained at 900 ºC (113 $m^2\ g^{-1}$). Fig. 1 shows that, in general, specific surface area in pores up to 100 Å (micro- and small mesopores) increases with temperature. The evolution of large mesopores (V_{meso}) and macropores (V_{macro}) is different, with a very pronounced decrease from 500 to 600 ºC, and low values in the 600–900 ºC range, with no clear trend (Table 2). This evolution of the porosity results in a decrease of the average pore size (D_p) with temperature.

Regarding the SCS-A series (acid washing after steam activation), the optimum values of both S_{BET} (323 $m^2\ g^{-1}$) and total pore volume V_{total} (0.553 $cm^3\ g^{-1}$) correspond to the activation temperature of 800 ºC. The highest value of S_{BET} represents about a three-fold increase compared to the best value of SCS series, with the advantage of the lower temperature required (800 ºC vs. 900 ºC). SCS-A-800 also possesses the highest value of micropore surface area S_{micro} (103 $m^2\ g^{-1}$, four times larger than the best value of SCS series). When comparing the data of SCS and SCS-A series, it is evident that the acid washing results in a significant enhancement of the porous structure at temperatures equal or higher than 600 ºC (for the temperature of 500 ºC there is little alteration). The values of S_{BET} of SCS-A samples are about 2–6 fold larger than the corresponding SCS samples. This increase in the pore area is observed in the whole pore range, but it is especially evident in the micro- and mesopore range. Consequently, it can be hypothesized that the acid washing is effective to make visible the pores generated during the pyrolysis that remain hidden due to pore blockage. The acid washing removes part of the material that blocks the porous structure, thus resulting in a better accessibility to pores. Thus, the acid washing with HCl is highly advisable to enhance the results of the pyrolysis with steam.

When analyzing the effect of the acid, it should be taken into account that the increase in the specific surface area may be due to the removal of inorganic matter (essentially non-porous). In this regard, the use of the corrected S_{BET} parameter has been proposed in the literature, as given by Eq. 1 [23]. This parameter does not take into account the contribution of the inorganic fraction to the S_{BET}:

$$Corrected\ S_{BET} = \frac{measured\ S_{BET}}{1 - ash\ content\ (mass\ fraction)} \quad (1)$$

Fig. 2 displays the corrected values of S_{BET}. As observed, the corrected values of S_{BET} of the samples subjected to acid washing after the steam activation are higher in the intermediate temperature range of 600–800 ºC. These results reflect that the improvement in the specific surface area (and consequently, in the porous structure of the material) is not only due to the mere removal of the inorganic fraction, but also to alterations in the porous structure. Contrarily, at both the lowest (500

Table 1
Data of overall yield of sludge carbon and partial yields of the different preparation steps (acid treatment and physical activation with steam), ash content and pH.

Sample	Y_{phys} (wt %)	Y_{acid} (wt %)	Y_{SC} (wt%)	Ash content (wt%)	pH
SCS-500	59.3	-	59.3	63.1	7.8
SCS-600	57.4	-	57.4	65.7	8.5
SCS-700	55.1	-	55.1	69.0	8.4
SCS-800	47.6	-	47.6	75.9	9.1
SCS-900	47.0	-	47.0	82.0	8.8
SCS-A-500	59.3	47.9	28.4	38.6	4.9
SCS-A-600	57.4	48.5	27.8	41.3	5.2
SCS-A-700	55.1	47.3	26.1	45.3	5.1
SCS-A-800	47.6	46.6	22.2	51.0	5.2
SCS-A-900	47.0	48.4	22.7	55.3	5.6
P-SCS-500	55.5	66.3	36.8	46.8	6.3
P-SCS-600	52.9	66.3	35.1	50.1	6.3
P-SCS-700	50.0	66.3	33.2	53.7	7.2
P-SCS-800	43.2	66.3	28.6	68.8	7.2
P-SCS-900	39.5	66.3	26.2	75.8	7.5

ºC) and the highest activation temperature (900 ºC), the values of SC and SCA samples are very similar.

The effect of the acid pretreatment (P-SCS series) is different depending on the activation temperature. At temperatures lower than or equal to 600 ºC, it has a detrimental effect, since there is an important decrease in both S_{BET} and pore area in all the pore size range (Table 2). This detrimental effect is also observed in the case of the corrected S_{BET} (Fig. 2). It is hypothesized that the removal of inorganic constituents before the thermal step would result in a lower extent of the reactions and processes occurring during the pyrolysis (such as the thermal decomposition of carbonates), thus leading to a lower generation of porosity. This negative effect would not be offset by the reactions favoured by the acid during the pyrolysis, owing to the low temperature employed (higher temperatures are required).

In contrast, the acid washing before steam pyrolysis has a beneficial effect at temperatures above 700 ºC. This positive effect can be observed in S_{BET}, with the maximum value corresponding to P-SCS-900 (179 m^2 g^{-1}, an increase of 58% compared to SCS-900). Nevertheless, the most visible effect of the prewashing is the enhancement of the micropore structure (Table 2), resulting in materials with high degree of microporosity. For example, S_{BET} increases around 58–63% for the acid pretreated samples (in the 700–900 ºC range) whereas the micropore area for these samples increases by around 270–450%. Regarding S_{micro} and S_{BET}, although the highest values correspond to the sample activated at 900 ºC, the sample activated at 800 ºC also exhibits suitable values (S_{BET} of 149 m^2 g^{-1} and S_{micro} of 94.5 m^2 g^{-1}), with the advantage of the lower temperature required. The acid pretreatment has also the effect of decreasing the meso- and macroporosity, compared to only physically activated samples (SCS). This effect in the porous structure results in a decrease in the pore size (26–36 Å for P-SCS samples activated at 700–900 ºC vs. 59–80 Å for SCS samples).

The data of Fig. 2 reveal that at 700 ºC the corrected S_{BET} of SCS and P-SCS samples is very similar, and it is below that of SCS-A-700. At higher temperatures (800–900 ºC), the values of P-SCS are higher than those of SCS, revealing that the improvement in the specific surface area is not only due to the removal of the inorganic fraction. At 800 ºC the corrected S_{BET} of SCS-A sample is still higher than that of P-SCS, whereas at the highest temperature (900 ºC) the value of P-SCS sample is the highest of all the samples. These results reveal that at temperatures lower than or equal to 800 ºC, the acid washing after the pyrolysis provides better results than the prewashing, likely due to the better accessibility of the acid to the interior or the particles, once the porous structure has been developed. On the contrary, the behaviour at 900 ºC suggests that higher temperatures are required for the occurrence of specific reaction mechanisms involving HCl (during the combined physical and chemical activation) that result in the development of the porous structure.

3.2.2. *Elemental analysis and concentration of heavy metals*

The results of the elemental analysis and the concentration of heavy metals for the precursor and selected samples of sludge biochars (samples prepared at 600 ºC) are shown in Table 3. The most abundant element, carbon, may be present in both inorganic constituents (such as carbonates) and organic constituents (e.g. aliphatic and aromatic hydrocarbons) [24]. Hydrogen mainly includes fatty and aromatic hydrogen, as well as hydrogen in functional groups [25]. The main source of nitrogen is biomass protein [20]. Regarding oxygen, it may appear in both inorganic compounds (e.g. carbonate and phosphate) and organic compounds (such as carboxyl and carbonyl) [20].

The carbon content of biochar (SCS-600) is lower than that of the precursor (21.9 vs. 29.7 wt%), in concordance with the results reported in the literature [17]. This decrease is attributed to the decomposition and volatilization of organic matter, along with other reactions such as carbon gasification. The carbon content remains constant after the acid washing (performed after the pyrolysis). This result reflects the occurrence of two opposite effects: (i) the removal of inorganic constituents, such as heavy metals, which leads to the concentration of carbon in the remaining matter, and (ii) the removal of carbon by HCl. The effect of the acid pre-washing is different, because it increases the amount of carbon. This result evidences the different extent of the aforementioned opposite effects, and reflects that the effect of the acid washing is different depending on the sequence. Regarding the oxygen content, it decreases when samples are subjected to acid treatment (either before or after the pyrolysis). This result may be explained by the removal of constituents such as carbonates or oxides by the acid.

Concerning the content of heavy metals, it is noteworthy that the pyrolysis with steam results in the concentration of metals (SCS-600 vs. the precursor), as a consequence of the removal of volatile matter. Ni metal constitutes an exception, since its concentration decreases during the physical activation. As will be discussed later (3.3.2. section), it is hypothesized that Ni is converted into nickel carbonyl $Ni(CO)_4$ through its reaction with CO (formed in the gasification of carbon). This compound is very volatile (boiling point of 43 ºC) and consequently, it would be released from the solid matrix.

When the sample prepared by steam pyrolysis is subjected to acid washing with HCl (SCS-A-600 vs. SCS-600), the most visible effect is the important reduction of Zn concentration (86%), as a result of its dissolution in HCl. It is also worth mentioning that, whereas the concentration of Ni and Cu increase after the acid washing (due to their concentration in the remaining matter), the concentration of Cr remains constant. This result suggests that the dissolution of Cr also takes place, although to a lesser extent.

Finally, when the acid washing is performed before the pyrolysis with steam (P-SCS-600), apart from the aforementioned processes (such as the formation of nickel carbonyl), of note is that the concentration of Cu decreases. This decrease is very significant, compared to both SCS-600 and SCS-A-600, and leads to a Cu concentration even lower than that of the precursor. This result evidences that the incorporated HCl is involved in the removal of Cu through a reaction mechanism that requires high temperature or heating, as will be discussed in 3.3.2. section.

3.2.3. *Surface morphology and chemical composition*

The SEM images of the analyzed biochars are depicted in Figures S1-S2 (Supplementary Material). Bone chars show heterogeneous surfaces with macroporosity. The prepared materials exhibit fractured and rough shapes. The samples prepared by steam pyrolysis possess similar grain size regardless of the heating temperature within the 500–900 ºC range

Table 2
Textural properties of sludge biochar. S, $m^2\ g^{-1}$; V, $cm^3\ g^{-1}$, D_p, Á.

	S_{BET}	S_{micro} [a]	S_{meso} [b]	S_{macro} [b]	V_{micro} [a]	V_{meso} [b]	V_{macro} [b]	V_{total} [c]	D_p [d]
SCS-500	45.1	6.90	9.74	26.0	0.00261	0.00768	0.169	0.179	106
SCS-600	40.3	9.23	28.9	1.54	0.00379	0.0768	0.0384	0.119	91.9
SCS-700	61.7	14.7	36.6	3.05	0.00635	0.0938	0.0738	0.174	80.1
SCS-800	93.4	25.4	50.7	3.63	0.0112	0.106	0.0885	0.206	63.7
SCS-900	113	20.9	64.6	2.22	0.00933	0.121	0.0491	0.179	59.0
SCS-A-500	33.0	5.22	20.1	4.45	0.00179	0.0667	0.0971	0.166	112
SCS-A-600	241	64.3	107	5.10	0.0287	0.205	0.105	0.339	52.5
SCS-A-700	250	29.8	172	5.10	0.0144	0.311	0.107	0.432	65.9
SCS-A-800	323	103	155	6.70	0.0455	0.374	0.133	0.553	65.8
SCS-A-900	266	59.9	129	8.30	0.0267	0.297	0.154	0.478	66.6
P-SCS-500	9.10	1.83	5.58	0.855	0.000618	0.0155	0.0214	0.0375	91.8
P-SCS-600	5.61	2.08	3.35	0.950	0.000943	0.0136	0.0266	0.0411	133
P-SCS-700	101	81.1	8.91	0.909	0.0351	0.0203	0.0233	0.0787	26.4
P-SCS-800	149	94.5	31.9	1.23	0.0412	0.0587	0.0300	0.130	33.3
P-SCS-900	179	98.9	45.0	1.78	0.0430	0.0814	0.0439	0.168	35.8

[a] t-plot method
[b] BJH method (adsorption branch)
[c] Sum of t-plot and BJH methods
[d] BET method

(Figure S1). However, in the highest magnification levels, surface roughness increases with temperature, particularly using temperatures of 700 ºC or higher. This enhanced roughness is likely to be responsible for the increased specific surface area of the latter samples, as indicated in Table 2. The acid treatment seems to increase macroporosity and the formation of dimples, especially when applied after the pyrolysis (Figure S2). Moreover, the acid treatment after the pyrolysis results in the development of abundant new pores. At higher magnification levels, the formation of surface irregularities and cracks becomes evident, consistent with the measured higher macropore volume in this series, compared to the acid pretreated sample (Table 2, 0.133 vs. 0.03 cm^3/g^{-1}).

The results of local EDX analyses confirm the high degree of heterogeneity of both the precursor (dry sewage sludge) and the analyzed samples of sludge biochar. In order to get a more accurate overview of surface composition, apart from the matrix, individual particles visible in surface were analyzed. The results are listed in Table 4. According to the results, the matrix of the samples prepared by steam pyrolysis (SCS) is rich in oxygen, calcium, iron and phosphorus, in good concordance with the composition of the precursor. Moreover, the matrix of the samples activated at temperatures above 700 ºC exhibits important amounts of Si and Al. The high amount of sulfur in the matrix of the precursor is noteworthy. This element appears in individual particles in samples activated at temperatures up to 700 ºC, forming species such as sulfates of Ca-Fe or Ba. Apart from the sulfates, other individual particles detected in SCS samples were identified as aluminosilicated agglomerates, oxides or carbonates of Ca, oxides of Fe, phosphates of Fe-Ca and SiO_2 (quartz).

Regarding the acid-treated samples, the matrix is rich in O, Fe, Si and Al, and low amounts of Ca and P are detected. In the sample prepared by acid-pretreatment (P-SCS-800) individual particles of phosphates of Fe-Ca were detected. The other individual particles are similar in both acid-treated samples: aluminosilicates, oxides of Fe and quartz.

3.2.4. *Crystalline structure*

The crystalline structure of the prepared sludge biochars was analyzed by means of XRD (Figure S3, Supplementary Material). The results reveal the highly amorphous nature of the samples. The identified structures are shown in Table 5. All samples exhibit the characteristic reflection peaks of SiO_2 (quartz), which was detected by EDX in several samples of sludge biochar (Table 4). According to the literature, quartz is the main component of ash, and its amount remains quite constant after HCl washing [6]. Muscovite, an aluminosilicate of K and Al ($KAl_2(AlSi_3O_{10})(OH)_2$) was also detected in every sample. The aluminosilicates detected in the acid-treated samples (SCS-A-800 and P-SCS-800) may be ascribed to this structure. Calcite ($CaCO_3$) is observed in samples non subjected to acid treatment, and activated under moderate temperatures (up to 700 ºC). It is well known that high temperatures result in the thermal decomposition of $CaCO_3$. Furthermore, it is concluded that the acid treatment (either before or after the steam pyrolysis) leads to its removal.

Regarding the formation of magnetite (Fe_3O_4), it is interesting to note that, in samples prepared by steam pyrolysis, high temperatures are required (it is only detected for SCS-900). Moreover, the acid washing (after the activation with steam) results in its removal. In contrast, magnetite is detected in every sample prepared by acid washing before the activation with steam (P-SCS). These results evidence that HCl favours reaction mechanisms that lead to the generation of magnetite, even at the lowest temperature studied (500 ºC). It is worth mentioning that the activation protocol used in this study (especially the procedure that includes the acid washing prior to the activation with steam) is effective to generate biochar with magnetic properties through the transformation of the Fe introduced during the water treatment process into magnetite, without adding a source of Fe. The presence of magnetite is an advantage for the reuse of sludge biochars in wastewater treatment, since magnetite favours the removal of anionic surfactants [26], phosphorus [27] and heavy metals such as lead, copper, zinc and manganese [28,29].

Apart from calcite, there are other crystalline structures that are only detected in SCS series: an aluminosilicate (microcline) and two phosphates (whitlockite and fluoroapatite). These structures are absent in the samples prepared by acid treatment, showing that they are removed by the acid. These results are in concordance with the literature. Indeed, it has been reported that the content of P and Al can be reduced by HCl washing [6].

When acid washing is performed after the steam activation (SCS-A series), apart from the aforementioned removal of certain structures (such as calcite and magnetite), new crystalline structures emerge: mordenite (an aluminosilicate), aluminium phosphate (only detected at the lowest temperature, 500 ºC), Co spinel ($CoAl_2O_4$, detected at the highest temperature) and diopside (a silicate, also detected at the highest temperature). These structures are absent in the samples prepared by acid pre-washing (P-SCS).

Finally, concerning the P-SCS series, the crystalline structure is significantly modified as a consequence of the acid pretreatment, and along with the absence of several structures (such as calcite or microcline), a new structure appears, zakharovite (a silicate). These results, together with the aforementioned generation of magnetite in the whole

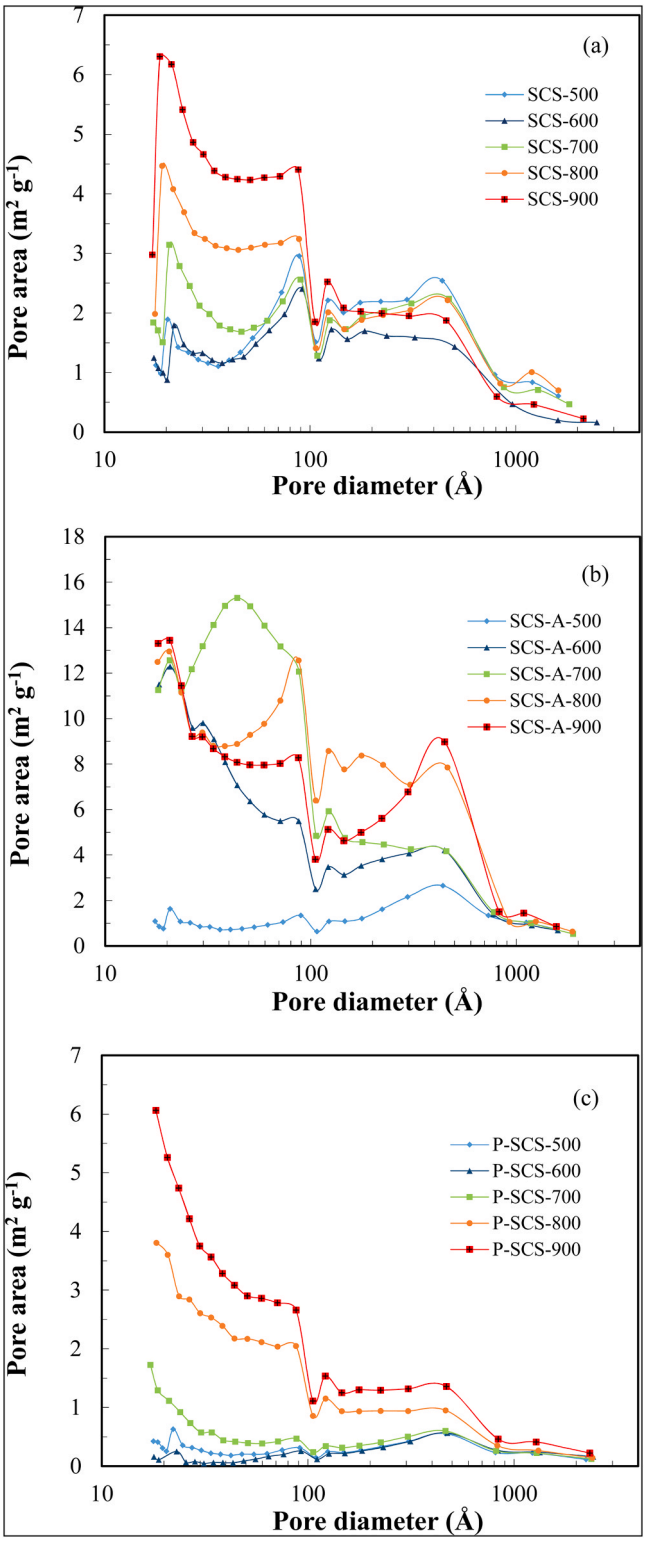

Fig. 1. Pore size distribution (PSD) of samples of sludge biochar. a) Samples prepared by pyrolysis with steam only. b) Samples prepared by pyrolysis with steam followed by acid treatment. c) Samples subjected to acid pretreatment followed by pyrolysis with steam.

temperature range, support the occurrence of reactions between the incorporated HCl and sludge constituents during the pyrolysis process.

3.2.5. *Surface functional groups*

Fig. 3 shows the FTIR spectra of the prepared samples of biochar, in order to get information about surface functional groups. Indeed, the thermochemical treatment may induce changes on biochar surface, such as the transformation of one functional group to another, the formation of new functional groups or the decomposition of the existing ones.

Concerning the samples prepared by steam pyrolysis only (Fig. 3a), the main band (located near 1030 cm^{-1}, peak I) is attributed to structures containing silicon, such as Si-O-Si and Si-O-X (X = C, Al, Fe, Ca, Mg

and Na) [30,31]. Moreover, every sample shows a set of peaks in the range of 400–800 cm^{-1}. Among them, the peaks between 600 and 800 cm^{-1} are likely due to the vibration of complex components of sludge carbon [31], whereas the bands below 600 cm^{-1} are believed to be related to the mineral content of sludge biochar (stretching vibration of M-X, where M is a metal and X a halogen) [5]. The band near 1420 cm^{-1} (peak II), which decreases with temperature, may be associated with different components that are thermally decomposed, such as long-chain aliphatic structures (C-H bending band), sulfates or carbonates [32]. The biochar prepared at 900 ºC shows almost no band, revealing that the removal of those compounds is almost complete. Possible surface functional groups are mainly carbonyl groups (C═O, associated with the shoulder near 1600 cm^{-1}, peak III) [30], and –OH and –NH groups (broad band with its maximum near 3400 cm^{-1}, peak IV) [33]. The oxygenated functional groups are generally related to the acidity of biochar [33]. The C═O band (peak III) shows a clear decreasing trend with temperature, as previously reported [13]. With regard to the broad band associated with -NH and –OH functionalities (peak IV, partially attributed to adsorbed water), the results evidence a decrease with temperature in the 500–700 ºC range, followed by a slight increase at higher temperature. This trend differs from the decreasing trend reported for other atmospheres, such as CO_2 and N_2 [13,33], and evidences the effect of the steam atmosphere on the generation of new functionalities, especially at high temperature. As discussed below (3.3.2. section), it is hypothesized that steam is involved in the generation of –OH groups.

When the samples activated with steam are subjected to acid washing (SCS-A series), there are several changes in the FTIR spectra. Fig. 3b shows that the peak related to the silicon content (peak I, 1030 cm^{-1}) is still the most prominent. Nevertheless, the shape and intensity of the bands below 600 cm^{-1} reveal changes in the mineral content of biochar. Indeed, the bands in the 530–600 cm^{-1} range undergo a substantial decrease, whereas those below 530 cm^{-1} appear better defined. The band near 1420 cm^{-1} (peak II) is also substantially altered. Indeed, whereas it is a clearly resolved peak in SCS series (with a decreasing trend with temperature), it appears as a weak shoulder after the acid treatment. This effect is associated with the removal of components such as $CaCO_3$ by HCl. Regarding surface functional groups, the results evidence that the acid treatment results in a modification of both –OH/-NH and C═O. In the case of C═O functionalities (shoulder near 1600 cm^{-1}, peak III), although the band exhibits the same decreasing trend with temperature as the SCS series, the decrease is less pronounced, and, in general, the intensity is higher after the acid washing, especially at temperatures above 700 ºC. The effect of the acid treatment on the broad band related to –OH and –NH functional groups (maximum close to 3400 cm^{-1}, peak IV) is different. The data show that the maximum intensity is obtained at 700 ºC. It is hypothesized that this result is a consequence of the aforementioned effects (the decrease of functional groups with temperature, and the generation of functional groups due to the steam atmosphere), along with the effect of the acid in the formation of functionalities. The effect of the acid treatment on the generation of C═O, -OH and -NH functionalities has been previously reported in the preparation of sludge biochar [13].

Fig. 3c shows the influence of the acid pretreatment on the FTIR spectra (P-SCS series). The band related to silicon (peak I) still shows the highest intensity. Moreover, the shape of the FTIR spectra in the region ascribed to the mineral content and to components such as long-chain aliphatic structures, sulfates or carbonates (at around 1400 cm^{-1}, peak II) is similar to those of the samples subjected to acid washing after the pyrolysis (SCS-A series). This result gives evidence on the effect of the acid in the removal of several constituents. Concerning the functional groups, the acid pretreatment results in an evolution of the C═O and –NH/-OH functionalities closer to that of SCS series. C═O functionalities (1600 cm^{-1}, peak III) exhibit a decreasing trend with temperature, more pronounced than that of SCS-A series. In the case of –NH/-OH functional groups (peak IV), there is a decrease with temperature up to 800 ºC. Then, a higher increase up to 900 ºC results in a similar intensity of the band, likely as a consequence of the generation of –OH groups by steam. In both SCS and P-SCS series, the highest intensity is obtained for the lowest temperature (500 ºC). Thus, the effect of the acid pretreatment in the generation of functionalities is less pronounced than that of the acid washing after the thermal treatment.

3.2.6. pH

With regard to the pH values, the samples prepared by pyrolysis with steam (SCS series) are basic in nature, with values of pH in the 7.8–9.1 range (Table 1). The acid treatment results in a decrease in the pH, more pronounced for the samples subjected to acid washing after the steam pyrolysis. In all series, the pH value increases with the activation temperature likely due to the thermal decomposition and/or desorption of acidic functional groups (C═O and –OH/-NH) [34,35], mainly C═O, as confirmed by FTIR analyses.

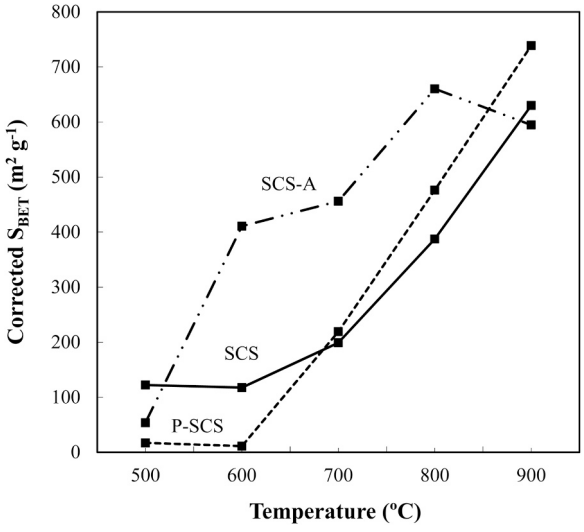

Fig. 2. Corrected values of BET specific surface area as a function of temperature.

Table 3
Results of elemental analysis and concentration of heavy metals of sewage sludge and sludge biochar. Elemental analysis, wt%. Heavy metals, mg kg^{-1}.

Sample	C	H	N	O	S	Cr	Ni	Cu	Zn	Pd
Precursor	29.7	4.1	3.2			167	586	376	3123	< 0.02
SCS-600	21.9	2.2	2.1	16.0	0.36	333	133	686	4558	< 0.7
SCS-A-600	21.9	2.1	2.1	7.8	1.05	336	190	901	638	< 0.7
P-SCS-600	37.2	2.4	3.5	7.0	0.11	322	119	336	1355	< 0.7

3.3. Investigation of the reactions and processes occurring during the activation

3.3.1. Thermal analysis of raw sewage sludge and acid impregnated sewage sludge

Fig. 4 shows the results of weight loss of sewage sludge under inert atmosphere (nitrogen) for raw sludge and sludge impregnated with HCl. It is observed that the sample subjected to acid pretreatment results in a higher mass loss (55.2 vs. 49.2 wt% up to 800 °C). The main difference in weight loss between both samples is obtained near 450 °C. At higher temperatures the mass loss of raw sludge is similar or higher than that of the acid treated sample.

The variation of mass can be divided into three stages: (i) low temperature, below 175 °C, (ii) intermediate temperature, 175–550 °C, and (iii) high temperature, above 550 °C. The first peak is attributed to moisture loss, and its amplitude is higher for the acid pretreated sample. The main loss of mass takes place in the intermediate temperature range, and involves several processes, since there are two overlapping peaks (near 290 and 330 °C for non-impregnated sludge) and a shoulder (near 450 °C). The DTG profile is similar to that reported by other authors [36,37]. The two overlapping peaks appear better defined and at slightly lower temperature for the acid pretreated sample, whereas the shoulder appears less marked. The processes that take place in this temperature range may include, the release of constitution water and the decomposition and volatilization of organic matter, among others. Specifically, the overlapping peaks near 300 °C have been attributed to the decomposition of aliphatic compounds, and the shoulder has been assigned to the decomposition of proteins and carbohydrates [38]. Regarding the mass loss at high temperature (above 550 °C), the well defined peak is mainly assigned to the thermal decomposition of mineral constituents such as $CaCO_3$ and sulfates. This peak is almost absent for the acid treated sample, revealing that an important removal took place during the acid impregnation.

3.3.2. Activation mechanism

The knowledge of the reactions and processes involved in the physicochemical activation of sewage sludge is considerably beneficial to prepare a material with optimal properties for the desired application. In this sense, in previous works several efforts have been made to investigate the activation mechanism in CO_2 atmosphere of raw sludge and sludge treated with alkalis [16]. Moreover, we have performed an extensive research on the activation mechanism of other carbonaceous precursors using different activating atmospheres and reagents (including acids) [39,40]. Thus, taking into account the results of those studies, along with the findings collected in the previous sections of this paper, a detailed activation mechanism has been proposed for raw sewage sludge and sludge treated with acid in steam atmosphere.

3.3.2.1. Raw sewage sludge. The following reactions and processes may take place during the physical activation of raw sewage sludge with steam, as discussed below: (i) the desorption of water, (ii) the decomposition and/or volatilization of constituents of the precursor (both organic and inorganic matter), (iii) carbon gasification reactions, (iv) the water gas shift reaction (Eq. (2)), (v) a set of reactions that involve the reaction of carbon constituent and OH^- ions, (vi) the formation of nickel carbonyl, and (vii) the formation of magnetite, Fe_3O_4. Except for the water gas shift (Eq. (2)), which takes place in gas phase, all reactions and processes involve gasification and, consequently, are expected to affect the textural properties of the solid matrix of the material.

$$CO + H_2O \leftrightarrow H_2 + CO_2 \quad (2)$$

As mentioned before (TG-DTG analysis), the thermal processes of water release and the volatilization/decomposition of organic matter take place at intermediate temperatures, up to 550 °C. Regarding the decomposition of inorganic matter, the aforementioned thermal decomposition of $CaCO_3$ (Table 5, XRD) should be highlighted, which occurs at temperatures above 700 °C [41]:

$$CaCO_3 \rightarrow CaO + CO_2 \quad (3)$$

The decomposition of sulfates is another thermal process that is worth mentioning. Among the sulfates detected by EDX (those of Ca, Fe and Ba), it is well documented that the thermal decomposition of iron (II) and iron (III) sulfates Eqs, (4) and (5) takes place at temperatures near 700 °C [42]. Both iron sulfates result in the production of Fe_2O_3. In contrast, higher temperatures (above 1100 °C) are required to produce the thermal decomposition of $CaSO_4$ and $BaSO_4$ [43,44]. Nevertheless, the data of EDX (Table 4) suggest that the removal of sulfates is complete at temperatures above 700 °C. In this regard, it should be taken into account that iron sulfates are expected to be the predominant sulfates (since they are added as coagulants in the purification of water), and thus, their removal by thermal decomposition would result in an almost complete removal of sulfates.

$$2\ FeSO_4 \rightarrow Fe_2O_3 + 2\ SO_2 + ½\ O_2 \quad (4)$$

$$Fe_2(SO_4)_3 \rightarrow Fe_2O_3 + 3\ SO_2 + \frac{3}{2} O_2 \quad (5)$$

Concerning the gasification of carbon, several reactions may occur. Among them, the following should be highlighted: (i) the reaction of carbon with steam, favoured by the steam atmosphere (Eq. (6)), and (ii) the reverse Boudouard reaction, that is, the reaction of carbon with CO_2 (Eq. (7)). Both reactions take place at high temperature, above 700 °C [39,45]. The CO_2 required for the reverse Boudouard reaction may come from the thermal decomposition of carbonates (Eq. (3)).

$$C + H_2O \rightarrow H_2 + CO \quad (6)$$

$$C + CO_2 \rightarrow 2\ CO \quad (7)$$

Another mechanism of interest is the reaction of carbon constituent of sewage sludge with OH^- ions. In this regard, two pathways are proposed. The first one implies the release of hydrogen [46]:

$$6\ OH^- + 2\ C \rightarrow 3\ H_2 + 2\ CO_3^{2-} \quad (8)$$

The second reaction pathway is based on the mechanism proposed by Robau-Sánchez et al. [47] (Eq. (9)). This mechanism results in the formation of cyanides, detected during the activation of raw sewage sludge in inert atmosphere [13,48]. Although the reactions proposed by Robau-Sánchez et al. require the reaction of gaseous N_2, in a previous paper it was concluded that structural nitrogen (constituent of the precursor) takes part as a source of nitrogen [39].

$$6\ OH^- + 5.5\ C + 2\ N \rightarrow 2\ (CN)^- + 2\ CO_3^{2-} + 1.5\ CH_4 \quad (9)$$

Eqs. (8) and (9) require the reaction of OH^- ions with sewage sludge constituents (carbon and nitrogen). OH^- ions, detected by means of FTIR

Table 4
Results of EDX analysis for selected samples of sludge biochar. Chemical composition (wt%).

Sample	Analyzed area	O	Ca	Fe	P	S	Al	Si	Ba	Mn	Zn	Pb	K	Mg	Ti	Au	Observations
Precursor	Matrix	**43.7**	**11.2**	**12.4**	**6.40**	**14.6**	2.40	3.34	-	-	-	-	-	-	-	-	
	IP1*	**60.5**	**34.6**	1.02	0.72	0.27	0.42	0.46	-	-	-	-	-	-	-	-	Oxides or carbonates of Ca
	IP2*	**53.1**	**5.47**	**23.2**	**11.0**	1.19	2.18	3.19	-	-	-	-	-	0.72	-	-	Phosphates of Fe-Ca
SCS-500	Matrix	**47.2**	**14.3**	**14.0**	**10.3**	1.55	4.37	**6.62**	-	-	-	-	0.25	0.54	0.40	-	
	IP1*	**48.6**	**6.09**	**7.90**	**5.19**	0.87	**7.92**	**19.8**	-	-	-	-	0.74	2.19	0.62	-	Aluminosilicated agglomerates
	IP2*	**65.8**	**29.5**	1.07	1.06	0.23	0.82	1.12	-	-	-	-	0.13	0.31	-	-	Oxides or carbonates of Ca
	IP3*	**43.5**	1.97	**37.6**	**15.9**	-	0.23	0.30	-	0.18	-	-	-	0.32	-		Phosphates of Fe
	IP4*	**69.3**	**5.42**	**5.60**	1.53	**12.5**	3.00	2.64	-	-	-	-	-	-	-	-	Sulfates of Ca-Fe
SCS-600	Matrix	**58.8**	**16.0**	**12.4**	**6.77**	0.89	2.68	1.80	-	-	-	-	-	0.42	-	-	
	IP1*	**32.8**	**64.4**	2.21	0.29	**-**	-	0.29	-	-	-	-	-	-	-	-	Calcium oxide
	IP2*	**59.4**	**15.9**	**10.8**	3.19	**8.06**	-	2.70	-	-	-	-	-	-	-	-	Sulfates of Ca-Fe
	IP3*	**29.7**	2.62	2.63	1.83	**12.0**	1.01	0.76	**49.5**	-	-	-	-	-	-	-	Barium sulfate
	IP4*	**46.3**	**5.41**	**6.84**	4.89	3.59	2.04	2.55	**-**	0.39	**27.2**	-	0.20	0.53	-	-	
	IP5*	**14.7**	1.82	**48.8**	0.72	4.17	**-**	0.77	-	1.27	**6.05**	**17.2**	-	-	-	-	Oxides of Fe with trace elements (Zn, Pb)
SCS-700	Matrix	**38.2**	**14.4**	**17.9**	**7.01**	0.83	**6.72**	**10.5**	**-**	**-**	**-**	-	1.72	0.60	-	-	
	IP1*	**-**	**5.04**	**92.6**	1.03	-	1.30	-	-	-	-	-	-	-	-	-	Nanometric tubular particles
	IP2*	**49.4**	**8.63**	**21.0**	**-**	**16.5**	2.41	2.02	-	-	-	-	-	**-**	**-**	**-**	Sulfates of Ca-Fe
	IP3*	**26.4**	1.81	**27.6**	1.02	0.24	**9.90**	**16.8**	-	0.46	-	**-**	**10.2**	2.58	2.59	**-**	
SCS-800	Matrix	**45.1**	**20.2**	**12.2**	**8.57**	-	**5.73**	**5.45**	-	-	-	-	0.43	0.65	0.32	-	
	IP1*	**53.5**	4.23	**5.96**	0.88	-	**11.2**	**18.4**	-	-	-	-	3.63	1.12	0.24	-	Microtubular or nanotubular particles
	IP2*	**40.4**	1.57	1.83	-	-	**11.8**	**37.47**	-	-	-	-	2.70	-	-	-	Aluminosilicates
	IP3*	**39.8**	3.43	**37.7**	**16.2**	-	1.25	0.74	-	-	-	-	-	1.03	-	-	Phosphates of Fe
SCS-900	Matrix	**36.5**	**18.9**	**16.6**	**9.58**	0.34	**5.86**	**9.43**	-	-	-	-	0.65	0.73	0.53	-	
	IP1*	**44.2**	**5.51**	0.64	0.61	-	**13.0**	**30.3**	-	-	-	-	1.39	-	-	-	Aluminosilicates
	IP2*	**46.3**	**7.19**	**29.8**	**12.1**	-	**-**	1.96	-	-	-	-	-	0.96	-	-	Phosphates of Fe-Ca
SCS-A-800	Matrix	**20.4**	1.95	**18.2**	1.31	2.24	**8.90**	**39.3**	-	-	-	-	3.27	-	1.05	-	
	IP1*	**42.7**	**-**	3.85	**-**	**-**	**17.3**	**26.8**	-	-	-	**-**	**9.32**	-	-	-	Aluminosilicates
	IP2*	**18.6**	0.50	**68.3**	**-**	0.48	1.99	**8.98**	-	-	-	-	0.44	0.70	-	-	Oxides of Fe with trace elements (Si)
	IP3*	**50.8**	0.53	**6.42**	**-**	0.90	1.67	**39.2**	-	-	-	-	0.46	-	-	-	Quartz
	IP4*	**-**	-	**-**	**-**	0.78	-	**-**	-	-	-	-	-	-	-	**91.4**	
P-SCS-800	Matrix	**39.4**	3.65	**12.6**	3.82	0.69	**7.12**	**25.4**	-	-	-	-	**5.21**	1.01	1.09	-	
	IP1*	**55.8**	-	-	-	-	-	**44.2**	-	-	-	-	-	-	-	-	Quartz
	IP2*	**48.2**	**21.1**	**13.9**	**11.1**	-	2.57	1.90	-	-	-	-	-	1.19	-	-	Phosphates of Fe-Ca
	IP3*	**49.7**	**-**	**6.63**	**-**	-	**9.09**	**28.8**	-	-	0.55	-	3.46	1.74	-	-	Aluminosilicates
	IP4*	**38.6**	0.95	**42.6**	1.13	-	3.43	**9.58**	-	-	0.12	-	2.31	0.96	0.38	-	Oxides of Fe with trace elements (Si)

* Individual particles visible in surface.

Table 5
Structures identified by XRD in sludge biochar.

Sample	Calcite ($CaCO_3$)	Quartz (SiO_2)	Muscovite	Microcline	Whitlockite	Fluorapatite	Magnetite	Aluminium phosphate	Mordenite	Spinel (Co)	Diopside	Zakharovite
SCS-500	Detected	Detected	Detected	Detected	-	-	-	-	-	-	-	-
SCS-700	Detected	Detected	Detected	Detected	Detected	-	-	-	-	-	-	-
SCS-900	-	Detected	Detected	Detected	Detected	Detected	Detected	-	-	-	-	-
SCS-A-500	-	Detected	Detected	-	-	-	-	Detected	Detected	-	-	-
SCS-A-700	-	Detected	Detected	-	-	-	-	-	Detected	-	-	-
SCS-A-900	-	Detected	Detected	-	-	-	-	-	-	Detected	Detected	-
P-SCS-500	-	Detected	Detected	-	-	-	Detected	-	-	-	-	Detected
P-SCS-700	-	Detected	Detected	-	-	-	Detected	-	-	-	-	Detected
P-SCS-900	-	Detected	Detected	-	-	-	Detected	-	-	-	-	Detected

analysis, may be formed from the hydration of oxides and/or carbonates (Eqs. (10)-(12)) [49,50]. The use of a steam atmosphere favours the occurrence of this set of reactions, as evidenced by the FTIR results (increase in OH^- functionalities at temperatures above 700 ºC).

$$O^{2-} + H_2O \rightarrow 2\ OH^- \quad (10)$$

$$CO_3^{2-} + H_2O \rightarrow HCO_3^- + OH^- \quad (11)$$

$$HCO_3^- \rightarrow OH^- + CO_2 \quad (12)$$

As mentioned before, the results of ICP (decrease in the concentration of nickel) suggest the formation of gaseous nickel carbonyl (Eq. (13)). $Ni(CO)_4$ is formed when metallic nickel contacts carbon monoxide at 70 °C [51]:

$$Ni + 4\ CO \rightarrow Ni(CO)_4 \quad (13)$$

The required carbon monoxide may be formed in several reactions and processes, such as the gasification of carbon with water and CO_2 (Eqs. (6) and (7)). Moreover, the role of carbon as a reducing agent of oxides and/or carbonates cannot be discarded (Eqs. (14) and (15)) [21].

$$O^{2-} + C \rightarrow CO \quad (14)$$

$$CO_3^{2-} + 2\ C \rightarrow 3\ CO \quad (15)$$

The XRD results evidence the presence of magnetite (Fe_3O_4) in the sample activated at the highest temperature (900 ºC), whereas it is absent for SCS-500 and SCS-700 samples (Table 5). Consequently, high temperatures are required for the generation of magnetite. Moreover, the steam atmosphere also plays an important role in the generation of magnetite, since in previous researches it was not detected in biochars prepared in CO_2 atmosphere, even at 900 ºC [16]. The formation of magnetite is believed to take place through the reaction of Fe^{3+} with OH^- ions. Two different pathways are proposed: (i) the direct formation of magnetite through the reaction of iron with hydroxides (Eq. (16)), and (ii) the formation of $Fe(OH)_3$ and its evolution to Fe_3O_4 (Eq. (17)), following a reaction scheme similar to that proposed in the literature for the formation of Fe_2O_3 [52].

$$3\ Fe^{3+} + 8\ OH^- + e^- \rightarrow Fe_3O_4 + 4\ H_2O \quad (16)$$

$$3\ Fe(OH)_3 + e^- \rightarrow Fe_3O_4 + 4\ H_2O + OH^- \quad (17)$$

The formation of $Fe(OH)_3$ may take place through: (i) the hydration with steam of the Fe_2O_3 oxide (Eq. (18)) formed through the aforementioned thermal decomposition of iron sulfates (Eqs. (4) and (5)), and (ii) the reaction of Fe^{3+} with hydroxides (Eq. (19)).

$$Fe_2O_3 + 3\ H_2O \rightarrow 2\ Fe(OH)_3 \quad (18)$$

$$Fe^{3+} + 3\ OH^- \rightarrow Fe(OH)_3 \quad (19)$$

The EDX results evidence the high iron content of the precursor (Table 4), which is a consequence of the addition of iron coagulants during the wastewater treatment process (iron (II) sulfate and/or iron (III) sulfate, in view of the high S content). Regarding the role of steam in the formation of magnetite, it is evident in Eq. (18). Moreover, the hydroxides required in Eqs. (16) and (19) may be formed through the aforementioned hydration reaction of oxides and/or carbonates (Eqs. (10)-(12)), and, consequently, the beneficial effect of steam is clear. The effect of temperature on the generation of magnetite appears in Eqs. (4) and (5). As mentioned before, temperatures higher than 700 ºC are required for the formation of Fe_2O_3 from iron sulfates, which would explain the requirement of high temperatures for the formation of magnetite.

3.3.2.2. Raw sludge subjected to acid washing after steam activation. The series of biochars prepared by acid washing after the activation with steam of raw sludge (SCS-A) has undergone the aforementioned reactions and processes during the activation with steam (Eqs. (2)-(19)). Moreover, the subsequent acid treatment with HCl results in the modification of the physicochemical properties of the materials.

As explained before, the acid washing after the steam treatment has the beneficial effect of unblocking the pores generated during the steam pyrolysis, thus making them accessible. Consequently, the acid treatment is advisable to maximize the results of the activation with steam. The dissolution of inorganic matter is likely to be the main pore unblocking mechanism. The data of XRD (Table 5) clearly show that $CaCO_3$ is among the compounds removed by the acid (Eq. (20)):

$$CaCO_3 + 2\ HCl \rightarrow CaCl_2 + CO_2 + H_2O \quad (20)$$

With regard to Fe oxides, although several oxides have been detected by EDX after performing the acid washing after the steam activation (SCS-A-800 in Table 4), the results of XRD (Table 5) show the removal of the magnetite (Fe_3O_4) generated at the highest temperature (900 ºC) (Eq. (21)), in concordance with the reported solubility of Fe_3O_4 in HCl [53].

$$Fe_3O_4 + 8\ HCl \rightarrow FeCl_2 + 2\ FeCl_3 + 4\ H_2O \quad (21)$$

Furthermore, the results of ICP-MS confirm the removal of Zn and Cr, that of Zn taking place to a greater extent. Both Zn and Cr may be part of many compounds, such as carbonates or oxides, thus resulting in

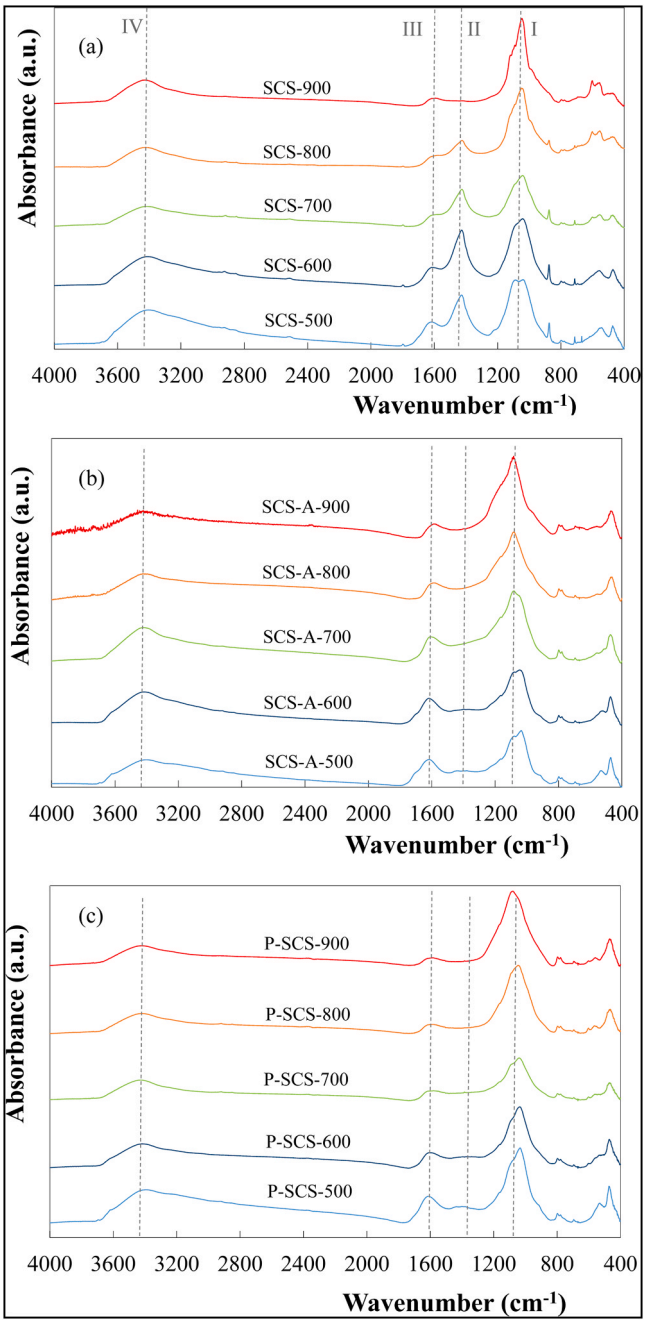

Fig. 3. FTIR spectra of samples of sludge biochar. a) Samples prepared by pyrolysis with steam only. b) Samples prepared by pyrolysis with steam followed by acid treatment. c) Samples subjected to acid pretreatment followed by pyrolysis with steam.

dissolution reactions similar to Eq. (22):

$$ZnO + 2\ HCl \rightarrow ZnCl_2 + H_2O \quad (22)$$

3.3.2.3. Sewage sludge impregnated with HCl before the steam activation. When raw sludge is impregnated with HCl before steam pyrolysis, on the contrary, the mechanisms that take place during the thermal treatment in steam atmosphere may be substantially modified, and additional reactions and processes may take place. Overall, the addition of a chemical reagent may have the following effects: (i) vaporization and/or thermal decomposition of the reagent, (ii) interaction of the reagent with the activating atmosphere (steam), (iii) interaction of the reagent with precursor constituents, and (iv) catalysis of several reactions. In this case, taking into account the nature of the precursor, the reagent and the atmosphere, (ii) and (iv) pathways have been discarded, and (iii) is believed to be the most important.

Several effects of the acid treatment before and after the steam activation are similar, namely, the removal of organic matter or inorganic constituents such as $CaCO_3$, Zn or Cr (Eqs. (20) and (22)) (ICP-MS and EDX, Tables 3 and 4). In this regard, as explained before, the excessive removal of several constituents by means of the acid pretreatment results in a lower extent of certain reactions and processes that take place during the pyrolysis (e.g. the thermal decomposition of calcite). This negative effect, which leads to a lower generation of porosity, is offset at high temperatures, since the acid impregnation before the steam activation results in the occurrence of additional reaction mechanisms, favoured at high temperatures.

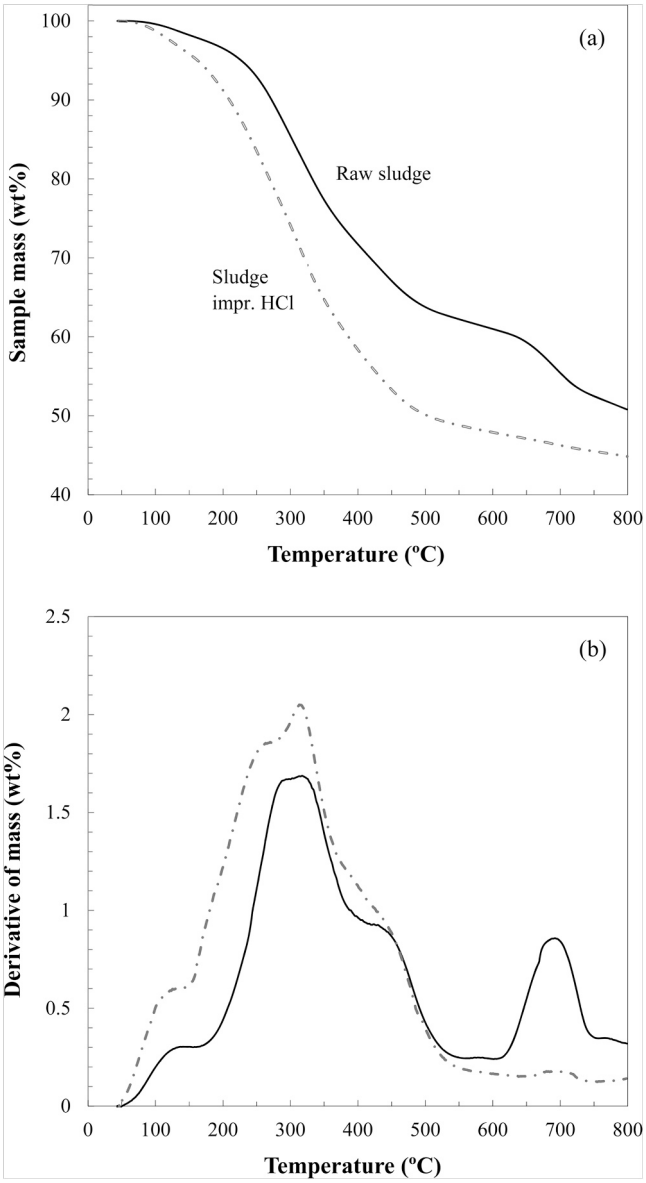

Fig. 4. Thermal behaviour under inert atmosphere of raw sewage sludge and sludge impregnated with HCl. a) TG curves. b) DTG curves.

Among those additional reactions, of interest is the aforementioned formation of magnetite in the whole temperature range (500–900 ºC), whereas for raw sludge high temperatures (900 ºC) are required to be formed (XRD, Table 5). Two hypotheses may explain the beneficial effect of the acid pretreatment on the generation of magnetite:

(i) Several mechanisms proposed for the generation of Fe_3O_4 involve the reaction of OH^- ions (Eqs. (16) and (19)), and the FTIR results show that the acid pretreatment increases their amount (likely by Eq. (23) followed by Eq. (12)):

$$CO_3^{2-} + H^+ \rightarrow HCO_3^- \quad (23)$$

The formation of bicarbonate (Eq. (23)) is believed to take place at intermediate temperature (around 400–500 ºC) [40] and thus, it would explain the generation of magnetite in the whole temperature range studied (500–900 ºC).

(ii) When magnetite is synthesized by co-precipitation (Eqs. (16)-(17) and (19)), iron chlorides are commonly used [29]. In this regard, the beneficial effect of the pretreatment with HCl in the formation of chlorides is clear. Fe may be part of many compounds, such as sulfates, phosphates or oxides (EDX, Table 4), and the formation of chlorides may take place through reactions similar to Eqs. (24)-(25):

$$FeSO_4 + 2\ HCl \rightarrow FeCl_2 + H_2SO_4 \quad (24)$$

$$Fe_2O_3 + 6\ HCl \rightarrow 2\ FeCl_3 + 3\ H_2O \quad (25)$$

Finally, the aforementioned reduction in Cu concentration should be highlighted (Table 3). As mentioned before, the concentration of Cu is not reduced with the acid washing after the steam activation, thus evidencing the absence of copper compounds such as CuO, Cu_2O and $CuCO_3$, which are soluble in HCl at room temperature [54]. In contrast, the prewashing followed by steam activation results in the decrease of the Cu amount. This result is in good concordance with previous results obtained in the preparation of sewage sludge biochar in CO_2 atmosphere [13], and reflects the role of the acid impregnation in the occurrence of additional reaction mechanisms that result in the removal of copper.

Among these reaction mechanisms, the formation of copper carbonyl may explain the reduction of the Cu amount. Although copper carbonyls are not the most usual carbonyl species, the formation of carbonyls has been reported at temperatures between 60 and 100 ºC during the interaction with CO of copper supported on a Y zeolite [55]. Cu(CO) is primarily formed and, with additional CO, the dicarbonyl is formed:

$$Cu(CO) + CO \rightarrow Cu(CO)_2 \quad (26)$$

Although some metal carbonyls can be formed from the direct reaction of the metal with carbon monoxide, such as Ni carbonyl (Eq. (13)), others are formed by the reduction of metal halides in the presence of carbon monoxide. In this regard, it is remarkable that in the aforementioned study, the catalyst was prepared by the impregnation of the zeolite support with CuCl [55]. Thus, the effect of the acid pretreatment on the formation of copper halides (chlorides, in this case) is clear. The copper chlorides formed are then involved in the generation of copper carbonyls during the thermal treatment.

4. Conclusions

The activation mechanism proposed for the pyrolysis of raw sewage sludge with steam includes the following reactions and/or processes that involve gasification: (i) the desorption of water, (ii) the decomposition and/or volatilization of constituents of the precursor (both organic and inorganic matter), (iii) carbon gasification reactions, (iv) reactions of carbon constituent with OH^- ions, (v) the formation of nickel carbonyl, and (vi) the formation of magnetite, Fe_3O_4. The formation of magnetite requires high temperatures (at least 900 ºC).

The effect of the acid treatment is different depending on the sequence (prior or after the pyrolysis with steam). The acid washing after the pyrolysis significantly enhances the porous structure due to pore unblocking, thus making visible the pores generated. The highest value of S_{BET} (323 $m^2\ g^{-1}$) represents a three-fold increase compared to samples subjected to steam pyrolysis only, with the advantage of the lower temperature required (800 ºC vs. 900 ºC). The drawback of the acid washing is the lower yield obtained (compared to the acid pretreatment), as well as the removal of magnetite, thus resulting in the loss of the magnetic properties of biochar.

The acid pretreatment has a detrimental effect in the development of porosity at temperatures up to 600 ºC, attributed to the removal of certain constituents, thus leading to a lower extent of the reactions and processes occurring during the pyrolysis. This effect is offset at temperatures above 700 ºC, due to the occurrence of additional reaction mechanisms involving the interaction of the impregnated HCl with sludge constituents. Apart from the increase in S_{BET}, the most visible effect of the pretreatment is the production of biochars with a high degree of microporosity, reflected in the average pore size, the lowest of the prepared materials. Among the reactions favoured by the acid, of interest is the development of magnetite in the whole temperature range studied.

The thermochemical treatment induces changes on biochar surface. The steam atmosphere is involved in the generation of –OH functionalities. The acid treatment results in the generation of C═O, -OH and -NH functionalities, the effect being more pronounced when the acid washing is performed after the steam pyrolysis.

The activation protocol used in this study (especially the procedure that includes acid washing prior to the pyrolysis with steam) is effective to generate biochar with magnetic properties through the transformation of the Fe introduced during the water treatment process, without adding a source of iron. The presence of magnetite is an advantage for the reuse of the prepared sludge biochars in wastewater treatment, since magnetite favours the removal of anionic surfactant, phosphorus and heavy metals such as lead, copper, zinc and manganese.

CRediT authorship contribution statement

Eva Epelde: Writing – review & editing, Investigation. **Irene Sierra:** Writing – original draft, Investigation, Formal analysis, Conceptualization. **Unai Iriarte-Velasco:** Writing – review & editing, Funding acquisition, Formal analysis. **Jose L Ayastuy:** Investigation, Funding acquisition.

Declaration of Competing Interest

The authors declare that they have no known competing financial interests or personal relationships that could have appeared to influence the work reported in this paper.

Data Availability

Data will be made available on request.

Acknowledgements

The authors wish to express their gratitude for the technical and human support provided by SGIker of UPV/EHU. Funding: This work was supported by the Basque Government (GV-2018-00038) and the Ministry of Science, Innovation and Universities of the Spanish Government (PID2022-140584OB-I00).

Appendix A. Supporting information

Supplementary data associated with this article can be found in the online version at doi:10.1016/j.jaap.2024.106545.

References

[1] A. Rorat, P. Courtois, F. Vandenbulcke, S. Lemiere, 8 - Sanitary and environmental aspects of sewage sludge management, in: M.N.V. Prasad, P.J. de Campos Favas, M. Vithanage, S.V. Mohan (Eds.), Industrial and Municipal Sludge, Butterworth-Heinemann, 2019, pp. 155–180, https://doi.org/10.1016/B978-0-12-815907-1.00008-8.

[2] Y. Chen, S. Li, S. Ho, C. Wang, Y. Lin, D. Nagarajan, J. Chang, N. Ren, Integration of sludge digestion and microalgae cultivation for enhancing bioenergy and biorefinery, Renew. Sust. Energ. Rev. 96 (2018) 76–90, https://doi.org/10.1016/j.rser.2018.07.028.

[3] J. Wang, S. Wang, Preparation, modification and environmental application of biochar: A review, J. Clean. Prod. 227 (2019) 1002–1022, https://doi.org/10.1016/j.jclepro.2019.04.282.

[4] P. Hadi, M. Xu, C. Ning, C. Sze Ki Lin, G. McKay, A critical review on preparation, characterization and utilization of sludge-derived activated carbons for wastewater treatment, Chem. Eng. J. 260 (2015) 895–906, https://doi.org/10.1016/j.cej.2014.08.088.

[5] A. Gopinath, G. Divyapriya, V. Srivastava, A.R. Laiju, P.V. Nidheesh, M.S. Kumar, Conversion of sewage sludge into biochar: a potential resource in water and wastewater treatment, Environ. Res. 194 (2021) 110656, https://doi.org/10.1016/j.envres.2020.110656.

[6] Y. Xiao, A. Raheem, L. Ding, W. Chen, X. Chen, F. Wang, S. Lin, Pretreatment, modification and applications of sewage sludge-derived biochar for resource recovery- A review, Chemosphere 287 (2022) 131969, https://doi.org/10.1016/j.chemosphere.2021.131969.

[7] J. Lehmann, S. Joseph, Biochar Environ. Manag. Sci. Technol., Earthscan, Lond. (2009), https://doi.org/10.4324/9781849770552.

[8] A. Zielińska, P. Oleszczuk, B. Charmas, J. Skubiszewska-Zięba, S. Pasieczna-Patkowska, Effect of sewage sludge properties on the biochar characteristic, J. Anal. Appl. Pyrolysis 112 (2015) 201–213, https://doi.org/10.1016/j.jaap.2015.01.025.

[9] G. Xu, X. Yang, L. Spinosa, Development of sludge-based adsorbents: Preparation, characterization, utilization and its feasibility assessment, J. Environ. Manag. 151 (2015) 221–232, https://doi.org/10.1016/j.jenvman.2014.08.001.

[10] M. Grifoni, F. Pedron, I. Rosellini, G. Petruzzelli, 26 - From waste to resource: sorption properties of biological and industrial sludge, in: M.N.V. Prasad, P.J. de Campos Favas, M. Vithanage, S.V. Mohan (Eds.), Industrial and Municipal Sludge, Butterworth-Heinemann, 2019, pp. 595–621, https://doi.org/10.1016/B978-0-12-815907-1.00026-X.

[11] I. Velghe, R. Carleer, J. Yperman, S. Schreurs, J. D'Haen, Characterisation of adsorbents prepared by pyrolysis of sludge and sludge/disposal filter cake mix, Water Res 46 (2012) 2783–2794, https://doi.org/10.1016/j.watres.2012.02.034.

[12] K.M. Smith, G.D. Fowler, S. Pullket, N.J.D. Graham, Sewage sludge-based adsorbents: A review of their production, properties and use in water treatment applications, Water Res 43 (2009) 2569–2594, https://doi.org/10.1016/j.watres.2009.02.038.

[13] I. Sierra, U. Iriarte-Velasco, M. Gamero, A.T. Aguayo, Upgrading of sewage sludge by demineralization and physical activation with CO_2: Application for methylene blue and phenol removal, Micro Mesopor. Mat. 250 (2017) 88–99, https://doi.org/10.1016/j.micromeso.2017.05.020.

[14] J.D. González, M.R. Kim, E.L. Buonomo, P.R. Bonelli, A.L. Cukierman, Pyrolysis of biomass from sustainable energy plantations: effect of mineral matter reduction on kinetics and charcoal pore structure, Energ. Source Part A. 30 (2008) 809–817, https://doi.org/10.1080/15567030600817878.

[15] J. Donald, Y. Ohtsuka, C. Xu, Effects of activation agents and intrinsic minerals on pore development in activated carbons derived from a Canadian peat, Mater. Lett. 65 (2011) 744–747, https://doi.org/10.1016/j.matlet.2010.11.049.
[16] I. Sierra, U. Iriarte-Velasco, J.L. Ayastuy, A.T. Aguayo, Production of magnetic sewage sludge biochar: investigation of the activation mechanism and effect of the activating agent and temperature, Biomass Convers. Biorefin. 13 (2023) 17101–17118, https://doi.org/10.1007/s13399-022-02372-w.
[17] J. Racek, J. Sevcik, T. Chorazy, J. Kucerik, P. Hlavinek, Biochar – recovery material from pyrolysis of sewage sludge: a review, Waste Biomass-.-. Valor 11 (2020) 3677–3709, https://doi.org/10.1007/s12649-019-00679-w.
[18] S. Singh, V. Kumar, D.S. Dhanjal, S. Datta, D. Bhatia, J. Dhiman, J. Samuel, R. Prasad, J. Singh, A sustainable paradigm of sewage sludge biochar: Valorization, opportunities, challenges and future prospects, J. Clean. Prod. 269 (2020) 122259, https://doi.org/10.1016/j.jclepro.2020.122259.
[19] G.Q. Lu, J.C.F. Low, C.Y. Liu, A.C. Lua, Surface area development of sewage sludge during pyrolysis, Fuel 74 (1995) 344–348, https://doi.org/10.1016/0016-2361(95)93465-P.
[20] Y. Chen, R. Wang, X. Duan, S. Wang, N. Ren, S. Ho, Production, properties, and catalytic applications of sludge derived biochar for environmental remediation, Water Res 187 (2020) 116390, https://doi.org/10.1016/j.watres.2020.116390.
[21] M. Hunsom, C. Autthanit, Adsorptive purification of crude glycerol by sewage sludge-derived activated carbon prepared by chemical activation with H_3PO_4, K_2CO_3 and KOH, Chem. Eng. J. 229 (2013) 334–343, https://doi.org/10.1016/j.cej.2013.05.120.
[22] C.H. Tessmer, R.D. Vidic, L.J. Uranowski, Impact of oxygen-containing surface functional groups on activated carbon adsorption of phenols, Environ. Sci. Technol. 31 (1997) 1872–1878, https://doi.org/10.1021/es960474r.
[23] A. Ros, M.A. Lillo-Ródenas, E. Fuente, M.A. Montes-Morán, M.J. Martín, A. Linares-Solano, High surface area materials prepared from sewage sludge-based precursors, Chemosphere 65 (2006) 132–140, https://doi.org/10.1016/j.chemosphere.2006.02.017.
[24] X. Xiao, B. Chen, Z. Chen, L. Zhu, J.L. Schnoor, Insight into multiple and multilevel structures of biochars and their potential environmental applications: a critical review, Environ. Sci. Technol. 52 (2018) 5027–5047, https://doi.org/10.1021/acs.est.7b06487.
[25] X. Xiao, Z. Chen, B. Chen, H/C atomic ratio as a smart linkage between pyrolytic temperatures, aromatic clusters and sorption properties of biochars derived from diverse precursory materials, Sci. Rep. 6 (2016) 22644, https://doi.org/10.1038/srep22644.
[26] O. Makarchuk, T. Dontsova, A. Perekos, A. Skoblik, Y. Svystunov, Magnetic mineral nanocomposite sorbents for wastewater treatment (Article ID), J. Nanomater. 2017 (2017) 8579598, https://doi.org/10.1155/2017/8579598.
[27] F. Liu, J. Zuo, T. Chi, P. Wang, B. Yang, Removing phosphorus from aqueous solutions by using iron-modified corn straw biochar, Front. Environ. Sci. Eng. 9 (2015) 1066–1075, https://doi.org/10.1007/s11783-015-0769-y.
[28] L. Giraldo, A. Erto, J.C. Moreno-Piraján, Magnetite nanoparticles for removal of heavy metals from aqueous solutions: synthesis and characterization, Adsorption 19 (2013) 465–474, https://doi.org/10.1007/s10450-012-9468-1.
[29] J. Ifthikar, J. Wang, Q. Wang, T. Wang, H. Wang, A. Khan, A. Jawad, T. Sun, X. Jiao, Z. Chen, Highly efficient lead distribution by magnetic sewage sludge biochar: sorption mechanisms and bench applications, Bioresour. Technol. 238 (2017) 399–406, https://doi.org/10.1016/j.biortech.2017.03.133.
[30] K.M. Smith, G.D. Fowler, S. Pullket, N.J.D. Graham, The production of attrition resistant, sewage–sludge derived, granular activated carbon, Sep. Purif. Technol. 98 (2012) 240–248, https://doi.org/10.1016/j.seppur.2012.07.026.
[31] J. Zou, Y. Dai, X. Wang, Z. Ren, C. Tian, K. Pan, S. Li, M. Abuobeidah, H. Fu, Structure and adsorption properties of sewage sludge-derived carbon with removal of inorganic impurities and high porosity, Bioresour. Technol. 142 (2013) 209–217, https://doi.org/10.1016/j.biortech.2013.04.064.
[32] A. Ros, M. Montes-Moran, E. Fuente, D.M. Nevskaia, M.J. Martin, Dried sludges and sludge-based chars for H_2S removal at low temperature: influence of sewage sludge characteristics, Environ. Sci. Technol. 40 (2006) 302–309, https://doi.org/10.1021/es050996j.
[33] C. Jindarom, V. Meeyoo, B. Kitiyanan, T. Rirksomboon, P. Rangsunvigit, Surface characterization and dye adsorptive capacities of char obtained from pyrolysis/gasification of sewage sludge, Chem. Eng. J. 133 (2007) 239–246, https://doi.org/10.1016/j.cej.2007.02.002.
[34] A. Méndez, G. Gascó, M.M.A. Freitas, G. Siebielec, T. Stuczynski, J.L. Figueiredo, Preparation of carbon-based adsorbents from pyrolysis and air activation of sewage sludges, Chem. Eng. J. 108 (2005) 169–177, https://doi.org/10.1016/j.cej.2005.01.015.
[35] M. Hofman, R. Pietrzak, NO_2 removal by adsorbents prepared from waste paper sludge, Chem. Eng. J. 183 (2012) 278–283, https://doi.org/10.1016/j.cej.2011.12.077.
[36] L. Nowicki, S. Ledakowicz, Comprehensive characterization of thermal decomposition of sewage sludge by TG–MS, J. Anal. Appl. Pyrolysis 110 (2014) 220–228, https://doi.org/10.1016/j.jaap.2014.09.004.
[37] W. Zuo, B. Jin, Y. Huang, Y. Sun, Thermal decomposition of three kinds of sludge by TG–MS and PY–GC/MS, J. Therm. Anal. Calorim. 121 (2015) 1297–1307, https://doi.org/10.1007/s10973-015-4651-8.
[38] W. Xiaohua, J. Jiancheng, Effect of heating rate on the municipal sewage sludge pyrolysis character, Energy Procedia 14 (2012) 1648–1652, https://doi.org/10.1016/j.egypro.2011.12.1146.
[39] U. Iriarte-Velasco, J.L. Ayastuy, L. Zudaire, I. Sierra, An insight into the reactions occurring during the chemical activation of bone char, Chem. Eng. J. 251 (2014) 217–227, https://doi.org/10.1016/j.cej.2014.04.048.
[40] I. Sierra, J.L. Ayastuy, M.A. Gutiérrez-Ortiz, U. Iriarte-Velasco, A study on the impact of the reaction mechanism of the thermochemical activation of bone char (by pyrolysis and carbonization), J. Anal. Appl. Pyrolysis 171 (2023) 105973, https://doi.org/10.1016/j.jaap.2023.105973.
[41] K.S.P. Karunadasa, C.H. Manoratne, H.M.T.G.A. Pitawala, R.M.G. Rajapakse, Thermal decomposition of calcium carbonate (calcite polymorph) as examined by in-situ high-temperature X-ray powder diffraction, J. Phys. Chem. Solids 134 (2019) 21–28, https://doi.org/10.1016/j.jpcs.2019.05.023.
[42] V. Petkova, Y. Pelovski, Comparative DSC study on thermal decomposition of iron sulphates, J. Therm. Anal. Calorim. 93 (2008) 847–852, https://doi.org/10.1007/s10973-008-9302-x.
[43] R. Kresse, U. Baudis, P. Jäger, H.H. Riechers, H. Wagner, J. Winkler, H.U. Wolf, Barium and Barium Compounds. Ullmann's Encyclopedia of Industrial Chemistry, Wiley, Weinheim, 2007, pp. 621–640, https://doi.org/10.1002/14356007.a03_325.pub2.
[44] Z. Wang, W. Yang, H. Liu, H. Jin, H. Chen, K. Su, Y. Tu, W. Wang, Thermochemical behavior of three sulfates ($CaSO_4$, K_2SO_4 and Na_2SO_4) blended with cement raw materials (CaO-SiO_2-Al_2O_3-Fe_2O_3) at high temperature, J. Anal. Appl. Pyrolysis 142 (2019) 104617, https://doi.org/10.1016/j.jaap.2019.05.006.
[45] N. Zong, Y. Liu, Learning about the mechanism of carbon gasification by CO_2 from DSC and TG data, Thermochim. Acta 527 (2012) 22–26, https://doi.org/10.1016/j.tca.2011.09.025.
[46] M.A. Lillo-Ródenas, D. Cazorla-Amorós, A. Linares-Solano, Understanding chemical reactions between carbons and NaOH and KOH, Carbon 41 (2003) 267, https://doi.org/10.1016/s0008-6223(02)00279-8.
[47] A. Robau-Sánchez, A. Aguilar-Elguézabal, J. Aguilar-Pliego, Chemical activation of Quercus agrifolia char using KOH: Evidence of cyanide presence, Micro Mesopor. Mat. 85 (2005) 331–339, https://doi.org/10.1016/j.micromeso.2005.07.003.
[48] I. Sierra, U. Iriarte-Velasco, E.A. Cepeda, M. Gamero, A.T. Aguayo, Preparation of carbon-based adsorbents from the pyrolysis of sewage sludge with CO_2. Investigation of the acid washing procedure, Desalin. Water Treat. (2015) 1–13, https://doi.org/10.1080/19443994.2015.1075428.
[49] C. Combes, S. Cazalbou, C. Rey, Apatite Biominerals, Minerals 6 (2016), https://doi.org/10.3390/min6020034.
[50] A. Yasukawa, K. Kandori, T. Ishikawa, TPD-TG-MS study of carbonate calcium hydroxyapatite particles, Calcif. Tissue Int. 72 (2003) 243–250, https://doi.org/10.1007/s00223-002-2032-3.
[51] G. Hayward, S. Baksa, Acoustic nickel carbonyl assay – proof of principle, Anal. Methods 5 (2013) 1708–1714, https://doi.org/10.1039/C3AY26250B.
[52] L. Tang, J. Yu, Y. Pang, G. Zeng, Y. Deng, J. Wang, X. Ren, S. Ye, B. Peng, H. Feng, Sustainable efficient adsorbent: Alkali-acid modified magnetic biochar derived from sewage sludge for aqueous organic contaminant removal, Chem. Eng. J. 336 (2018) 160–169, https://doi.org/10.1016/j.cej.2017.11.048.
[53] mindat.org and the Hudson Institute of Mineralogy, Magnetite, 2024.
[54] J. Zhang, H.W. Richardson, Copper Compounds. Ullmann's Encyclopedia of Industrial Chemistry, Wiley, Weinheim, 2016, pp. 1–31, https://doi.org/10.1002/14356007.a07_567.pub2.
[55] H. Miessner, H. Landmesser, N. Jaeger, K. Richter, Surface carbonyl species of copper supported on dealuminated Y zeolite, J. Chem. Soc, Faraday Trans. 93 (1997) 3417–3422, https://doi.org/10.1039/A702959D.